energies

MDPI

Article

Enhancing Power Supply Flexibility in Renewable Energy Systems with Optimized Energy Dispatch in Coupled CHP, Heat Pump, and Thermal Storage

Dongwen Chen [1,2] and Zheng Chu [2,*]

[1] College of Information Science & Electronic Engineering, Zhejiang University, Hangzhou 310058, China; dongwenchen@sjtu.edu.cn
[2] School of Information and Electrical Engineering, Hangzhou City University, Hangzhou 300015, China
* Correspondence: chuz@hzcu.edu.cn; Tel.: +86-21-34206056

Abstract: The use of renewable energy by converting it into heat is an important form of storing energy in a usable form and improving the energy supply flexibility; therefore, the electricity–heating system (EHS) can cope with load fluctuations. However, relevant research is lacking on improving the energy supply limitations by the optimal dispatch of energy flow at the typical EHS, such as the coupled CHP–heat pump–thermal storage system (CCHTS). Based on the study of the energy supply characteristics of the CCHTS for extending the energy supply limitation, this study develops an optimal dispatch method using a heat pump (HP) and the thermal storage (TS) of heating networks to improve the flexibility of the CCHTS and the accommodation capacity of renewable energy. The maximum and minimum energy supply limitation model of the CCHTS and the output power characteristic model are established. Based on the piecewise power supply constraint, the energy flow of the EHS is optimized by using the quadratic programming algorithm. The CCHTS can significantly improve the energy supply flexibility; both coupled combined heat and power (CHP) + HP and coupled CHP + TS can improve the power supply flexibility, but the enhanced effect of CHP + HP is better than that of CHP + TS. An increase of 7.6% in wind power consumption is achieved. The consumption of renewable energy increases by 17.9% in the energy flow optimization results.

Keywords: power supply flexibility; thermal storage; renewable energy accommodation; power supply limitations; tightly coupled flexible thermal power system; thermal inertia

Citation: Chen, D.; Chu, Z. Enhancing Power Supply Flexibility in Renewable Energy Systems with Optimized Energy Dispatch in Coupled CHP, Heat Pump, and Thermal Storage. *Energies* **2024**, *17*, 2861. https://doi.org/10.3390/en17122861

Academic Editor: Stéphane Grieu

Received: 26 April 2024
Revised: 3 June 2024
Accepted: 10 June 2024
Published: 11 June 2024

1. Introduction

A low-carbon society requires a large-scale consumption of renewable energy [1,2]. However, the fluctuation and uncertainty of renewable energy electricity (REE) impact the power grids and general energy systems [3]. The electricity–heating system combines the power grid and heating networks, improves its power supply flexibility through the coupling between different equipment, and has the potential to a achieve large-scale consumption of renewable energy [4,5].

CHP is one of the core energy conversion equipment in the EHS. By improving the limits of the heat-to-power ratio and increasing the power supply flexibility, the renewable energy electricity accommodation in the EHS can be effectively improved [6,7]. However, in the winter heating season, CHP generally operates in the mode of "supply power determined by heating". The power supply flexibility is, therefore, reduced [8]. And then the accommodation of REE for the EHS is not effective, resulting in the significant curtailment of REE [9,10].

By introducing energy storage, the power supply flexibility of CHP can be effectively improved. Battery or electric vehicles are also typical forms of energy storage used in electric power systems [11]. For example, through the scheduled discharging of electric vehicles, an optimal scheduling strategy is proposed to enable renewable energy consumption [12].

Moreover, other forms of energy storage, such as P2G with CHP units, can be used for the integrated electricity–gas systems to respond to uncertainties [13]. However, the high electricity storage cost hinders its integration in power grids. Since the thermal storage (TS) cost is far lower than the electricity storage cost, previous research mainly concentrated on TS [14–16]. For example, the CHP-based district heating network (DHN) with an REE and TS system was studied, and a modeling and optimization method was developed [14]. Through the combination of an HP and TS, the production cost was minimized in [15] and the profit was maximized in [16]. Through an electrical boiler with TS, the system flexibility is improved and the wind curtailment is reduced by 12% [17]. Considering their dynamic response, TS tanks are used to improve REE consumption [18]. Using the TS storage in DHNs by artificial-neural-network-based forecasting models, the gas-fired CHP plant can better cope with load fluctuations [19]. These works have helped to improve the energy supply flexibility [19]; however, adding additional TS equipment to the energy system will lead to a significant increase in construction costs, which is economically unfeasible. In addition, the additional TS equipment experiences significant heat loss during the process of heat storage and release [20].

The heat transfer medium and buildings have a large heat capacity, which can flexibly store heat and reduce heat loss. Since the heat capacity of DHNs can be used to replace TS effectively, power supply flexibility can be realized [21,22]. For example, by using the thermal inertia of the heat capacity of buildings, an optimal and flexible dispatch method can be obtained [23–27]. By utilizing the thermal inertia of residential buildings, the economic performance is improved [28,29] and flexible electric power regulation is obtained [30]. The flexibility performance can be further improved by using the thermal inertia of DHNs [31–34]. In summary, using the thermal inertia of DHNs can promote the consumption of the REE. However, when the heat storage capacity of the DHN is relatively small compared to the power load of the grid, the use of the DHN's thermal inertia to improve the flexibility or adaptability of REE is not significant. Introducing electricity–heat energy conversion equipment can further improve the flexibility of the power grid in order to achieve the consumption of REE.

Moreover, energy conversion is another useful method for improving power supply flexibility. The heat pump, as an efficient form of heating equipment, can operate flexibly and co-operate with TS to further improve the flexibility of the EHS [35]. In previous studies, there has been some research on the flexible regulation of HPs. For example, through a hybrid HP and a TS unit, a residential building was able to operate flexibly, and the operation costs were reduced [36,37]. HPs with a flexible operation can realize load shifting, thereby improving the REE consumption and the efficiency of dispatch power plants [38]. To compensate for fluctuating REE and to avoid grid congestion, the demand–response service is provided by electric-to-heating equipment [39]. However, it has not been found that the HP was used in the EHS, combined with the heat capacity of the DHN and CHP, to improve the power supply flexibility of the whole EHS and, therefore, improve the consumption of the REE.

In summary, from the perspective of the initial investment, heat storage with the same energy storage capacity is much cheaper than batteries [14–16]; from the perspective of the operating costs, the operation of thermal storage equipment mainly relies on the circulation pump to drive the heat transfer medium for the heat exchange. The lifespan of the thermal storage equipment is not related to the number of thermal storage/heat release cycles, but only to the calendar lifespan; the operating cost of the batteries is related to the number of cycles [40,41]. Thermal storage is usually better than other energy storage devices. In this study, thermal storage and HPs are used to improve the performance of the EHS.

Based on the above literature reviews, this study develops an optimal dispatch method using an HP and TS of a DHN to improve the flexibility of the CCHTS and to improve the renewable energy accommodation capacity. The contributions are summarized as follows:

(1) New System Construction: For the first time, a new EHS was constructed by introducing HPs in order to achieve a more flexible energy supply. In the new EHS, CHP

and HPs are two complementary energy conversion devices forming a new electricity–heating energy supply regulation unit, the combined unit (CU). Compared to the optimal scheduling studies of EHSs in [24,26,29,31], the new system can adjust the output between electricity and heating by the adjustable heat-to-power ratio of the heat pump.

(2) Coupling Characteristics Indices: Studying the segmented electricity–heating output characteristic curve of HPs, the coupling characteristics relationship between CHPs and HPs in EHS systems are proposed for the first time, and detailed indices of the IES with coupling HPs are derived, including the maximum electrical power output (EPO), minimum EPO, and dispatch flexibility index of the IES. Compared to [31], the electricity–heating coupling characteristics model of CHP is expressed as a piecewise linear function; therefore, the overall model belongs to a quadratic programming model, and the modeling complexity and solution difficulty are reduced. The model belongs to a quadratic programming problem and has a unique solution, so it can be solved using any quadratic programming solver.

(3) Model Exploration and Performance Evaluation: A new system dispatch method coupling models of HPs with CHP is developed, and then the energy supply boundary is extended and the flexibility of the EHS and the consumption of REE is enhanced. Compared with references [39], the new model not only considers the coupling between HPs and power grids but also considers the coupling between HPs and CHP.

A comparison of the modeling characteristics of key equipment in the EHS is shown in Table 1.

Table 1. A comparison of modeling characteristics of key equipment in the EHS.

References	Heat Storage in Heating Pipelines	Electricity–Heating Characteristics of CHP	Characteristics of CHP Coupling HP	Electricity–Heating Characteristics of CHP Coupling HP
[24,26]	√	×	×	×
[29,31]	√	√	×	×
[39]	×	×	√	×
This study	√	√	√	√

This paper is organized as follows. Detailed models, including the TS model of the DHN, are presented in Section 2. The collaborative dispatch (CD) method of the EHS is provided in Section 3. The flexibility indices of the combined unit (CU) and the flexibility assessment model of the EHS are presented in Section 4. Two types of network topological case studies are proposed in Section 5. Finally, the conclusions are presented in Section 6.

2. Modelling of the DHN

2.1. Description of the Heating System

Due to the great heat capacity of water, DHNs are heat energy storage systems with massive potential in hot water in heating pipelines. The operation mode of "constant mass flow" is adopted more and more widely. The constant mass flow mode is adopted. Usually, the waste heat generated by equipment such as CHP and thermal power generation units serves as a heat source to generate heat for external heating. The detailed structure of the DHN is shown in Figure 1.

The heat generated by CHP is transmitted to the heat exchanger by the circulating hot water in primary pipelines. Typically, the TS loss in the secondary pipe is much smaller than in the primary pipe. The characteristics of heat loss and heat transmission delay are only considered in the primary pipe networks in this study.

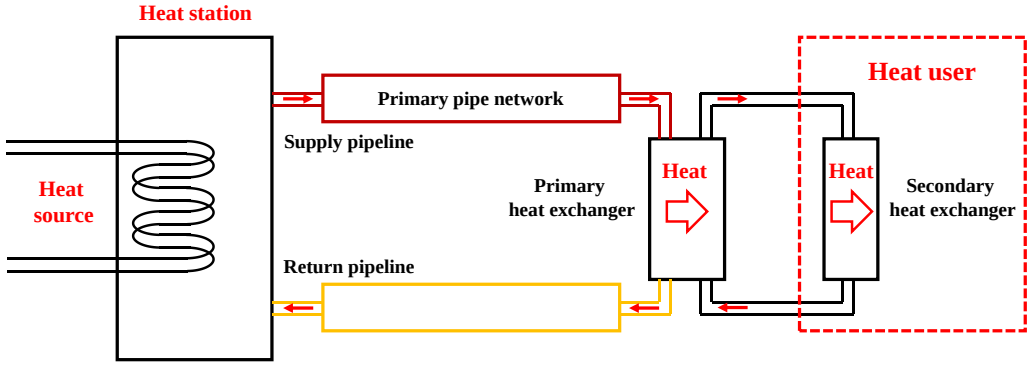

Figure 1. Schematic diagram of DHN.

2.2. Description of the Heat Sources

For CHP, the generated electricity is injected into the electricity networks, while the generated heat supplies the heat users through the primary and secondary pipe networks. There are four corner points in the feasible operation region. The heating power output (HPO) and EPO of the extreme point i are defined as x_i^k and y_i^k. The generated electrical power and heat power are coupled at any time; any co-ordinate point responding energy generated within the polyhedral operation region can be described by a convex combination of four extreme points. A detailed example of the electricity–heating coupling characteristics is shown in Figure 2 [30].

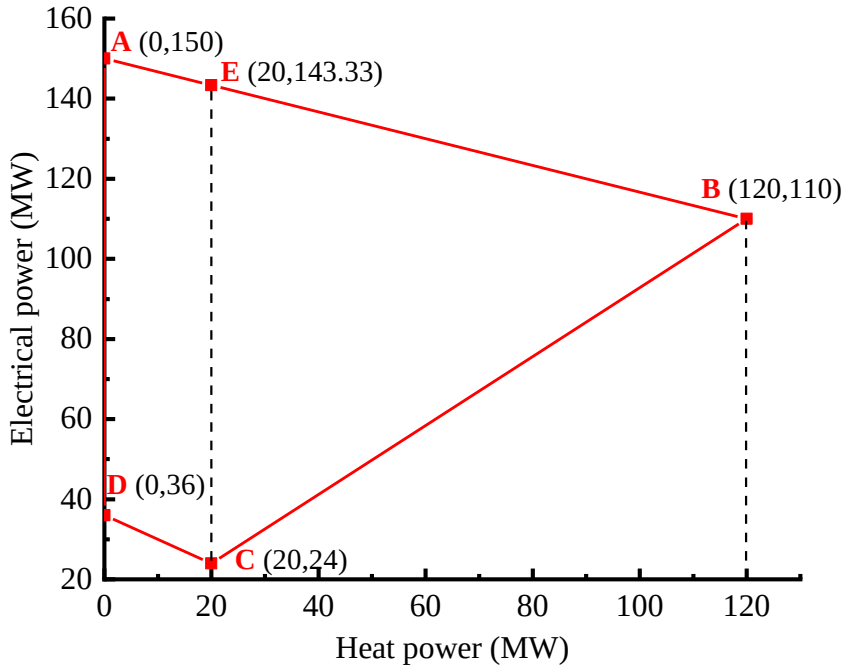

Figure 2. Electricity–heating coupling characteristics of CHP.

The relationship between the EPO P_{it}^{CHP}, the heating power output Q_{it}^{CUP}, and the corner co-ordinates are:

$$\begin{cases} P_{it}^{CHP} = \sum_{k=1}^{Ni} \alpha_{it}^k y_{it}^k \\ Q_{it}^{CHP} = \sum_{k=1}^{Ni} \alpha_{it}^k x_{it}^k \end{cases}, \forall i \in N_{CHP} \quad (1)$$

The parameters of N_i and α_{it}^k satisfies the constraints:

$$\begin{cases} \sum_{k=1}^{N_i} \alpha_{it}^k = 1 \\ 0 \le \alpha_{it}^k \le 1 \end{cases}, \forall i \in N_{CHP}, k \in \{1, 2, \cdots, N_i\} \quad (2)$$

2.3. Modelling of the DHN

The mass flow of each pipeline is assumed to be constant. Heat users can adjust the heat exchange area of the heat exchanger to adjust the return water's temperature. For the steady state, all state properties do not change along with the time during the period. The steady model can be shown as [42]:

$$\Phi = C_w m_q (T_{su} - T_{re}) \quad (3)$$

where C_w is the specific heat capacity of the water; m_q is the mass flow rate; T_{su} and T_{re} are the temperatures of the supply water and return water, respectively; and Φ is the heating load.

For the steady state, the HPO is determined by Equation (4) [42]:

$$\Phi_i^{CHP} = C_w m_q^{HS} \left(T_{su}^{HS} - T_{re}^{HS} \right), \forall i \in\in N_{HS} \quad (4)$$

During the storing or releasing of heat energy, the temperature changes with time, and the primary pipe networks are in an unsteady state. The HPO is determined by Equation (5):

$$\begin{cases} \Phi_i^{CHP} = C_w m_q^{HS} \frac{\int_{t-\Delta t}^{t} \Delta T^{HS}(t) dt}{\Delta t} \\ \Delta T^{HS} = C_w m_q^{HS} \left(T_{su}^{HS} - T_{re}^{HS} \right) \end{cases} \quad (5)$$

When the time Δt, the dispatch time interval, is short enough, assuming the temperature changes linearly, Equation (6) can be obtained:

$$\Phi_i^{CHP}(t) = C_w m_q^{HS} \left[\Delta T^{HS}(t) + \Delta T^{HS}(t - \Delta t) \right] / 2 \quad (6)$$

Considering that the time transmission delay (TTD) is long enough from the heat sources to the users and heat sources, the temperature change cannot be transmitted from the supply water to the return water during the time interval Δt. When the user loads remain constant, the return temperature is [25]:

$$T_{re}^{HS}(t) \approx T_{re}^{HS}(t - \Delta t) \quad (7)$$

Then, the temperature change is:

$$\Delta T^{HS}(t) = \Delta T^{HS}(t - \Delta t) + \left[T_{su}^{HS}(t) - T_{su}^{HS}(t - \Delta t) \right] \quad (8)$$

Therefore, the HPO is calculated as:

$$\Phi_i^{CHP}(t) = C_w m_q^{HS} \left[T_{su}^{HS}(t - \Delta t) - T_{re}^{HS}(t - \Delta t) \right] + \frac{C_w m_q^{HS} \left[T_{su}^{HS}(t) - T_{su}^{HS}(t - \Delta t) \right]}{2} \quad (9)$$

Equation (9) consists of two parts: the heat transferred from the input to the output of the pipeline, and the heat absorbed by the pipeline's hot water.

The first law of thermodynamics can also apply to heat exchangers. The heat power is [31]:

$$\Phi_i^{HE} = C_w m_q^{HE} \left(T_{su}^{HE} - T_{re}^{HE} \right), \forall i \in\in N_{HE} \quad (10)$$

At the mixing node, the laws of heat power conservation and mass flow conservation are applicable. The process can be expressed for both the supply and return water as [31]:

$$\begin{cases} \sum\limits_{inflows} (T_{su,in} \cdot m_{su,in}) = T_{su,out} \cdot \sum\limits_{inflows} m_{su,i} \\ \sum\limits_{inflows} (T_{re,in} \cdot m_{re,in}) = T_{re,out} \cdot \sum\limits_{inflows} m_{re,i} \end{cases} \tag{11}$$

Figure 3 shows the schematic diagram of the topology structure of the secondary hot water supply pipeline, as well as the temperature and its changes with different pipes at the inlet and outlet of the supply and return pipelines at the convergence node. Several different mass flows of hot water are injected into the same node, and then mixed. $T_{su,in}$ is the hot water's inlet temperature in the supply pipeline before injecting the node; $T_{su,out}$ is the hot water's outlet temperature in the return pipeline after mixing at the node; $m_{su,in}$ and $m_{su,out}$ are the inlet mass flow and outlet mass flows of the supply pipe networks, respectively; and $m_{re,in}$ and $m_{re,out}$ are the inlet mass flow and outlet mass flows of the return pipe networks, respectively.

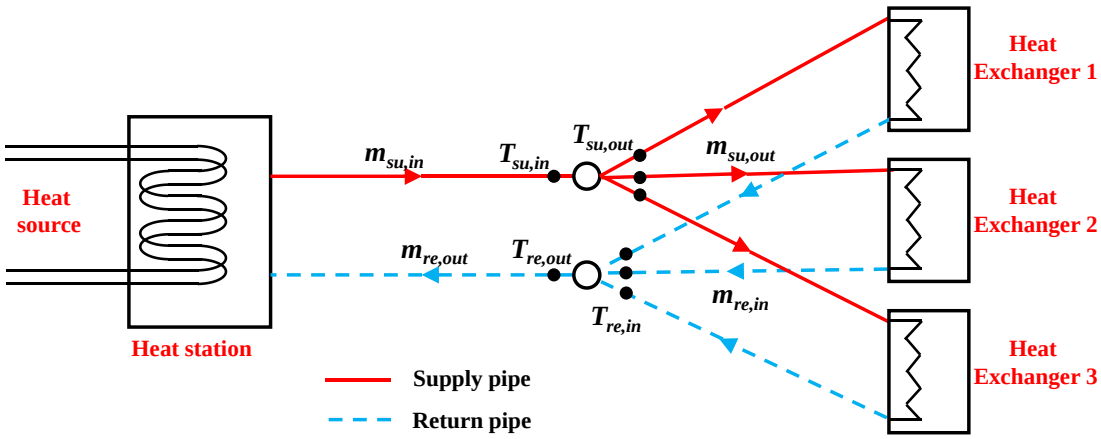

Figure 3. Structural diagram of the DHNs.

The temperature constraints are required for both the steady-state operation and unsteady-state operation. The constraints are expressed as:

$$\begin{cases} T_{i,su,\min} \le T_{i,su}(t) \le T_{i,su,\max} \\ T_{i,re,\min} \le T_{i,re}(t) \le T_{i,re,\max} \end{cases} \tag{12}$$

The characteristics of TTD and the TS capability of DHNs originating from the great heat capacity of primary pipe networks indicate that the DHNs have thermal inertia. The effect of the TS capability of DHNs is shown in Equation (9).

After absorbing the heat energy from the heat station, the hot water medium flows into the primary heating pipe networks' supply pipeline. The circulating pump results in velocity v, so temperature changes at the inlet pipeline have the TTD effect. The TTD, t_{delay}, is calculated as [28,29]:

$$t_{delay} = k_{delay} \frac{L}{v} \tag{13}$$

where k_{delay} is the thermal delay coefficient, and L is the pipeline's length. Considering the dispatch time interval, Equation (13) can be further expanded as [28,29]:

$$t_{delay} = round\left(\frac{k_{delay} \cdot L}{v \cdot \Delta t}\right) \cdot \Delta t \tag{14}$$

where *round*() is the rounding function.

The temperature decrease in the heating pipeline resulting from the heat transmission loss can be calculated by:

$$\begin{cases} T_{end} = T_{am} + (T_{start} - T_{am}) \cdot k_e \\ k_e = e^{-\frac{\lambda_0 L}{C_w m_q}} \end{cases} \tag{15}$$

where T_{am} is the ambient temperature, which can be assumed to be the constant that equals the average temperature of the soil.

The coefficient, λ_0, is calculated as [42]:

$$\lambda_0 = \frac{2\pi\lambda}{\ln \frac{D+2\delta}{D}} \tag{16}$$

where δ is the thermal insulation material's thickness, λ is the thermal insulation materials' thermal conductivity; and D is the inner diameter.

When considering both the heat transmission loss and TTD, Equation (15) can be extended as:

$$T_{end}(t) - T_{am}(t) = \left[T_{start}(t - t_{delay}) - T_{am}(t - t_{delay})\right] \cdot k_e \tag{17}$$

For two nodes that are not adjacent, the TTD of the temperature is:

$$\begin{cases} t_{delay,i,j} = t_{delay,i,k} + t_{delay,k,j} \\ T_i(t - t_{delay,i,j}) - T_{am}(t - t_{delay,i,j}) = \left[T_k(t - t_{delay,i,k}) - T_{am}(t - t_{delay,i,k})\right] \cdot k_{e,i,k} \\ T_k(t - t_{delay,k,j}) - T_{am}(t - t_{delay,k,j}) = \left[T_j(t - t_{delay,k,j}) - T_{am}(t - t_{delay,k,j})\right] \cdot k_{e,k,j} \end{cases} \tag{18}$$

where i, k, and j are sequential nodes along the flow direction.

2.4. Modelling of the User Heating Loads

For the walls, the thermal equilibrium equation is [23,25]:

$$\begin{cases} C_{w,j}\dfrac{dT_{w,j}}{dt} = \displaystyle\sum_{s \in N_j^w} \frac{T_{s,j} - T_{w,j}}{R_{w,j}} + r_j \alpha_j A_j^w Q_j^{rad} \\ r_j = \begin{cases} 1, \ exposed\ to\ the\ sunlight \\ 0, \ otherwise \end{cases} \end{cases} \tag{19}$$

where $C_{w,j}$ is the jth wall's heat capacity; $T_{w,j}$ is the jth wall's temperature; $T_{s,j}$ is the adjacent nodal temperature; $R_{w,j}$ is the thermal resistance; α_j is the heat-absorbing coefficient; Q_j^{rad} is the radiative heat flux density; and A_j^w is the area.

For the room, the thermal equilibrium equation is [23,24]:

$$\begin{cases} C_{z,i}\dfrac{dT_{z,j}}{dt} = \displaystyle\sum_{s \in N_i^w} \frac{T_{w,j} - T_{z,i}}{R_{w,j}} + \pi_k \sum_{s \in N_i^w} \frac{T_{c,j} - T_{z,i}}{R_{window}} + Q_i^{\text{int}} + Q_{R,i} + \pi_k \tau_j^w A_j^{window} Q_j^{rad,window} \\ \pi_k = \begin{cases} 1, \ there\ is\ a\ wall\ between\ nodes\ i\ and\ j \\ 0, \ otherwise \end{cases} \end{cases} \tag{20}$$

where $C_{z,i}$ is the ith room's heat capacity; $T_{z,j}$ is the ith room's temperature; $T_{c,j}$ is the ambient temperature; τ_j^w is the jth wall's heat transfer resistance; R_{window} is the thermal resistance of the windows; and A_j^{window} is the jth wall's whole area of the window.

The heating power from the heat exchangers is [31]:

$$\Phi_j = \frac{1}{\eta_{HE}} \sum_{i=1}^{N_{building}} Q_{R,i} \tag{21}$$

where η_{HE} is the efficiency of the heat exchanger; and $N_{building}$ is the number of buildings.

The TS of the building can be used to provide the appropriate temperature change:

$$T_{z,i}^{\min} \le T_{z,i}(t) \le T_{z,i}^{\max} \tag{22}$$

where $T_{z,i}^{min}$ and $T_{z,i}^{max}$ are the minimum and maximum limits, respectively.

3. Collaborative Dispatch Model of EHS

The proposed method provides power supply flexibility for the EHS by fully utilizing the TS of DHNs and buildings; therefore, the reduction in wind power (WP) curtailment can be achieved.

3.1. Objective Functions

The coal consumption of CHP and traditional thermal power units is considered. The objective of the optimization model is [26,27]:

$$\min C_{sum} = \Delta t \cdot \sum_{t=1}^{T} \left(\sum_{G_i \in S_{CG}} F_{Gi} + \sum_{g_i \in S_{CHP}} F_{gi} + \sum_{w_i \in S_{wi}} F_{wi} \right) \tag{23}$$

where Δt is the dispatch time interval; F_{Gi}, F_{gi}, and F_{wi} are the costs of the traditional thermal power, CHP, and WP. F_{Gi}, F_{gi}, and F_{wi} can be further described as [26,27]:

$$\begin{cases} F_{Gi} = a_{Gi} P_{Gi}^2 + b_{Gi} P_{Gi} + c_{Gi}, \ \forall Gi \in S_{CG} \\ F_{gi} = a_{1,gi} P_{gi}^2 + b_{1,gi} P_{gi} + a_{2,gi} H_{gi}^2 + b_{2,gi} H_{gi} + b_{3,gi} P_{gi} H_{gi} + c_{gi}, \ \forall Gi \in S_{CHP} \\ F_{wi} = \delta_{wi} \cdot \left(P_{wi}^{forecast} - P_{wi} \right), \ \forall wi \in S_{wi} \end{cases} \tag{24}$$

where a_{Gi}, b_{Gi}, and c_{gi} are the coal cost coefficients, respectively; $a_{1,gi}$, $a_{2,gi}$, $b_{1,gi}$, $b_{2,gi}$, $b_{3,gi}$, and c_{gi} are the economic operation parameters; P_{gi} is the output power of traditional thermal power units; P_{gi} and H_{gi} are the output electrical power and heating power, respectively; P_{wi} is the utilized WP; $P_{wi}^{forecast}$ is the forecasted WP; and δ_{wi} is the penalty cost coefficient.

3.2. Constraints

The constraint of the nodal power balance in electricity networks is expressed as [26,28]:

$$\vec{P}(t) + \vec{P_W}(t) - \vec{D}(t) = \vec{B} \times \vec{\theta}(t) \tag{25}$$

where $\vec{P}(t)$, $\vec{P_W}(t)$, and $\vec{D}(t)$ are the vectors of the EPO of CHP, WP, and the user electricity load during the period t; B is the nodal admittance matrix; and $\theta(t)$ is the phase angle.

The electrical power constraint is [26,28]:

$$-P_{ij}^{\max}(t) \le \frac{\theta_i(t) - \theta_j(t)}{x_{ij}} \le P_{ij}^{\max}(t) \tag{26}$$

where $P_{ij}^{max}(t)$ and $-P_{ij}^{max}(t)$ are the power limits; $\theta_i(t)$ and $\theta_j(t)$ are the phase angles at nodes i and j during the period t; and x_{ij} is the reactance of the feeder. The phase angle of the reference bus is set to 0:

$$\theta_{ref} = 0 \tag{27}$$

The phase angle constraints at node i are:

$$\theta_{i,\min}(t) \le \theta_i(t) \le \theta_{i,\max}(t) \tag{28}$$

The active EPO constraint is:

$$P_{Gi,\min} \le P_{Gi}(t) \le P_{Gi,\max} \tag{29}$$

The ramping constraints of CHP and the thermal power units are [26,28]:

$$\begin{cases} Ramp_k^{down} \cdot \Delta t \le P_k(t) - P_k(t-\Delta t) \le Ramp_k^{up} \cdot \Delta t \\ Ramp_k^{H,down} \cdot \Delta t \le H_k(t) - H_k(t-\Delta t) \le Ramp_k^{H,up} \cdot \Delta t \end{cases} \tag{30}$$

where k is the kth thermal power unit or CHP; $Ramp_k^{down}$ and $Ramp_k^{up}$ are the rates of ramp-down and ramp-up of the generators; and $Ramp_k^{H,down}$ and $Ramp_k^{H,up}$ are the rates for CHP. The total electrical power and heating power is the generation dispatch of CHP or the thermal power units with a dispatch period.

The EPO and HPO of CHP are:

$$\begin{cases} P_{i,\min}^{CHP}(t) \le P_i^{CHP}(t) \le P_{i,\max}^{CHP}(t) \\ Q_{i,\min}^{CHP}(t) \le Q_i^{CHP}(t) \le Q_{i,\max}^{CHP}(t) \end{cases}, \forall i \in N_{CHP} \tag{31}$$

The EPO limit of the WP generator is:

$$0 \le P_{w,i}(t) \le P_{w,i}^{forecast}(t) \tag{32}$$

where $P_{w,i}^{forecast}(t)$ is the forecasted WP output of the WP generator i during period t.

The dispatch model of EHS is solved by the QUADPROG solver in MATLAB R2018b software.

4. Flexibility Assessment

4.1. Flexibility Indices of the Combined Unit of CHP and HP

Higher-proportion CHP and renewable power generation bring tremendous challenges to the dispatch of the energy system. Flexibility indices are proposed to assess the flexibility improvement for the integrated energy system.

By introducing HPs into the CHP system, surplus electricity can be used for heating during the period of peak heating consumption and low power consumption, to improve the heating capacity. Considering the TS of the DHN, the CU can convert the surplus electricity into heat through HPs during the low heat consumption period, and store it in the heating network. By releasing the heat during the heat consumption peak, the flexibility of the whole CU for supplying electricity can be improved.

4.1.1. Maximum EPO of the CU

When introducing HPs into the CHP system, the electrical power–heat coupling characteristics of the CU are changed.

On the one hand, the heating power of HPs is limited by the COP:

$$0 \le Q^{HP} \le COP \cdot P^{HP} \tag{33}$$

where Q^{HP} is the output heating power of the HP; and P^{HP} is the consumed electrical power of the HP.

On the other hand, since the function of the HP in the combined system is to preheat the supply water of CHP, there is a maximum constraint on the heat-to-power ratio of the HP to that of CHP:

$$0 \le \frac{Q^{HP}}{Q^{CHP}} \le k_{HP-CHP} \tag{34}$$

Figure 4 shows the power output variation in the electricity–heating coupling characteristics of CHP.

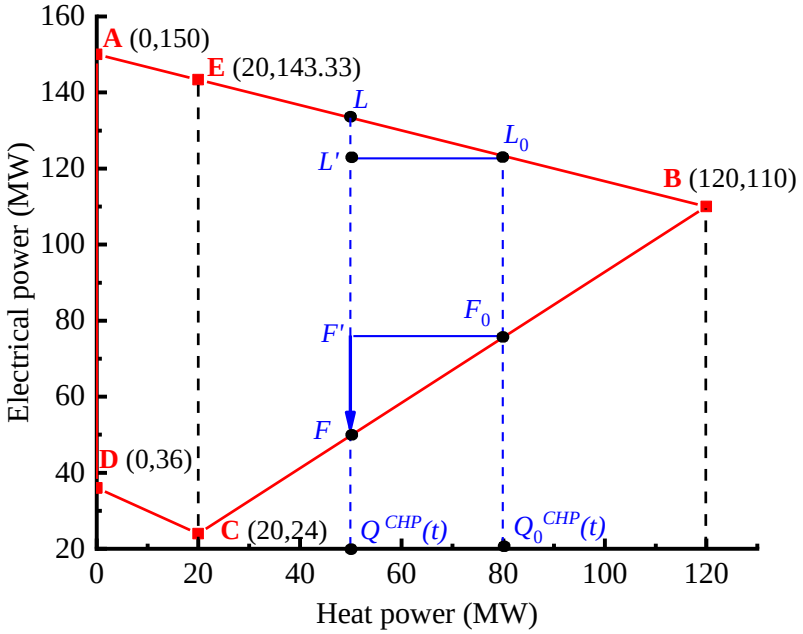

Figure 4. Power output variation in the electricity–heating coupling characteristics of CHP.

According to Figure 4, the maximum EPO meets the constraints:

$$\left(P^{CHP}\right)_{\max} = 150 - \frac{1}{3}Q^{CHP} \tag{35}$$

When considering the electricity consumed by HPs, the maximum EPO is:

$$\left(P^{CU}\right)_{\max} = \left(P^{CHP} - P^{HP}\right)_{\max} = \left(150 - \frac{1}{3}Q^{CHP} - P^{HP}\right)_{\max} = 150 - \frac{1}{3}Q^{CHP} - \left(P^{HP}\right)_{\min} \tag{36}$$

The HP can consume electricity but cannot generate electricity; therefore, the maximum EPO or the minimum electricity consumption is zero. The maximum EPO of the IES is the same as that of CHP:

$$\begin{cases} \left(P^{CU}\right)_{\max} = 150 - \frac{1}{3}Q^{CHP} - \left(P^{HP}\right)_{\min} = 150 - \frac{1}{3}Q^{CHP} = \left(P^{CHP}\right)_{\max} \\ \left(P^{HP}\right)_{\min} = 0 \end{cases} \tag{37}$$

4.1.2. Minimum EPO of the CU

The EPO of the IES is the algebraic sum of the EPO of CHP and the HP. Therefore, the minimum EPO of the IES is:

$$\left(P^{CU}\right)_{\min} = \left(P^{CHP} - P^{HP}\right)_{\min} = \left(P^{CHP}\right)_{\min} - \left(P^{HP}\right)_{\max} \tag{38}$$

The minimum EPO of the CHP is:

$$\left(P^{CHP}\right)_{\min} = \begin{cases} 36 - 0.6Q^{CHP}, & 0 \le Q^{CHP} \le 20 \\ 6.8 + 0.86Q^{CHP}, & 20 \le Q^{CHP} \le \left(Q^{CHP}\right)_{\max} \end{cases} \tag{39}$$

For the HP, the maximum HPO is constrained by the maximum electrical power consumption of the HP and the available ratio of the heating power of the HP to that of CHP:

$$\left(Q^{HP}\right)_{\max} = COP \cdot \left(P^{HP}\right)_{\max} = \min\left\{COP \cdot P^{HP}_{rated},\ k_{HP-CHP} \cdot Q^{CHP}\right\} \tag{40}$$

Considering the rated maximum HPO of the HP is:

$$\left(Q^{HP}\right)_{\max,rated} = COP \cdot P^{HP}_{rated} \tag{41}$$

Then, the maximum HPO can be further expressed as:

$$\left(P^{HP}\right)_{\max} = \min\left\{P^{HP}_{rated}, \frac{k_{HP-CHP} \cdot Q^{CHP}}{COP}\right\} \tag{42}$$

Therefore, the minimum EPO of the IES about Q^{CHP} is concluded and obtained as:

$$\left(P^{CU}\right)_{\min} = \left(P^{CHP}\right)_{\min} - \min\left\{P^{HP}_{rated}, \frac{k_{HP-CHP} \cdot Q^{CHP}}{COP}\right\} \tag{43}$$

Considering the whole HPO is:

$$Q = Q^{HP} + Q^{CHP} \tag{44}$$

Combining the maximum HPO of the HP and the minimum EPO of the IES about Q^{CHP}, the minimum EPO of the IES about the whole HPO is:

$$\left(P^{CU}\right)_{\min} = \begin{cases} 36 - \frac{Q}{1+k_{HP-CHP}}\left(0.6 + \frac{k_{HP-CHP}}{COP}\right), & 0 \le Q \le 20 \cdot (1 + k_{HP-CHP}) \\ 6.8 + \frac{Q}{1+k_{HP-CHP}}\left(0.86 - \frac{k_{HP-CHP}}{COP}\right), & 20 \cdot (1 + k_{HP-CHP}) \le Q \le \frac{(1+k_{HP-CHP})COP \cdot \mathrm{P}^{HP}_{rated}}{k_{HP-CHP}} \\ 6.8 + 0.86Q - (0.86COP + 1) \cdot \mathrm{P}^{HP}_{rated}, & Q \ge \frac{(1+k_{HP-CHP})COP \cdot \mathrm{P}^{HP}_{rated}}{k_{HP-CHP}} \end{cases} \tag{45}$$

4.1.3. Flexibility of the CU

In the DHN, we assume that the initial HPO is Q^0_{CHP} (t), and the coupling EPO range is line L_0F_0. When CHP is combined with TS, its HPO decreases from $Q^0_{HSsu,}(t)$ to $Q^{CHP}(t)$. Correspondingly, the EPO range extends from L_0F_0 to LF. Compared to the initial EPO, CHP obtains the larger capability of EPO (LL' and FF'), which are called CHP's flexibility.

Based on the maximum and minimum EPO of the CU, the electrical power–heat coupling characteristics of the CU are obtained and shown in Figure 5.

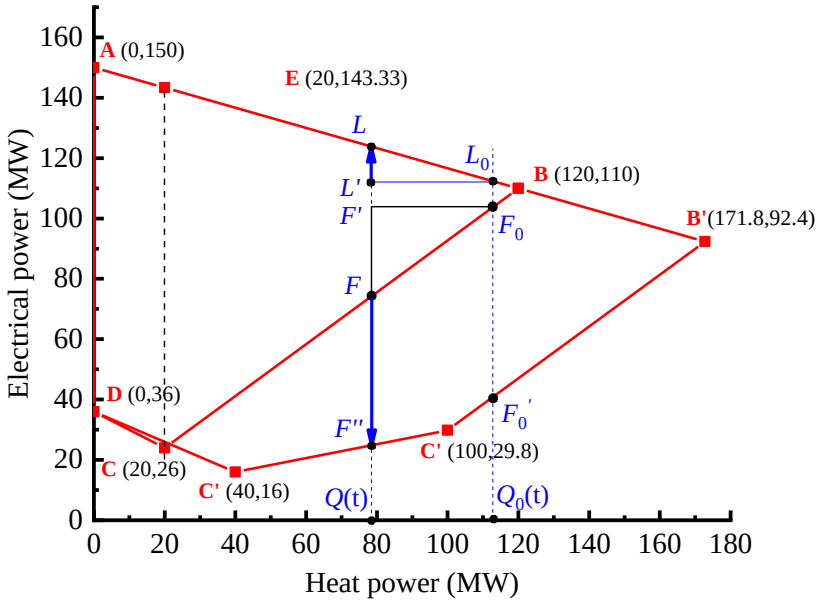

Figure 5. Electrical power–heat coupling characteristics of the CU.

In Figure 5, the part marked in the black polygon is the changed part of the electrical power–heat coupling characteristics curve of the IES relative to CHP due to the addition of HPs. Compared with the flexibility of CHP, the added flexibility of the IES is line FF''. Compared to the initial EPO, the IES obtains the further capability of the EPO, LL' and FF'', which is called IES's flexibility.

The HPO change is described as:

$$\Delta Q(t) = Q_0(t) - Q(t) = \min\left[\Delta t \cdot Ramp_k^{H,down},\ \Delta t \cdot (Q_{\max}(t) - Q(t))/2,\ Q_S(t)\right] \quad (46)$$

where $Q_{\max}(t)$ is the maximum HPO of the IES; $Q(t)$ is the output heat energy of DHNs and buildings; and $Q_S(t)$ is the sum of the heat energy storage of DHNs and buildings:

$$Q_S(t) = C_w m_q^{HS}\left[T_{su}^{HS}(t) - T_{su,\min}^{HS}\right] + C_{wall} M_{wall}\left[T^{wall}(t) - T_{\min}^{wall}\right] \quad (47)$$

where $T_{su,\min}^{HS}$ is the minimum temperature of the supply water for the heat sources, IES; M_{wall} is the total mass of the walls of buildings; $T^{wall}(t)$ is the wall's temperature; and $T_{\min}^{wall}$ is the lower-limit temperature of the wall.

4.2. Flexibility Indices

The flexibility of the electrical power system, including the upward flexibility and downward flexibility, is described as [31]:

$$\begin{cases} f^{down}(t) = \sum_{i=1}^{N} \min\{\Delta t \cdot r_{i,down},\ [P_i(t) - P_{i,\min}(t)]\} \\ f^{up}(t) = \sum_{i=1}^{N} \min\{\Delta t \cdot r_{i,up},\ [P_{i,\max}(t) - P_i(t)]\} \end{cases} \quad (48)$$

where $f^{up}(t)$ and $f^{down}(t)$ are the upward and downward flexibility reserves for the combined CHP and the traditional thermal power units; $r_{i,down}$ and $r_{i,up}$ are the ramp rates of unit i; and $P_{i,\max}(t)$ and $P_{i,\min}(t)$ are the extrema of the active EPO.

4.3. Flexibility Assessment Models

Based on CHP's flexibility indices, the accumulated upward/downward flexibility model is:

$$\begin{cases} f_{DOWN} = \sum_{t=1}^{T_{down}} f^{down}(t) \\ f_{UP} = \sum_{t=1}^{T_{up}} f^{up}(t) \end{cases} \quad (49)$$

where T is the hours of valley/peak periods.

4.4. Flow Chart

Based on the previous DHNs' models and building models, the EHS dispatch model, and related flexibility indices, the flowchart is shown in Figure 6.

According to Figure 6, the process is as follows:

(1) Based on the EHS parameters, models of DHNs considering thermal characteristics of both TS and temperature TTD are established (Equations (1)–(18)). The remaining models of the integrated EHSs, including models of electricity networks and buildings, are further established (Equations (19)–(22)).

(2) The objective function is established for optimal dispatch. The objective is to minimize the daily operation cost of the EHS (Equations (23) and (24)). And the constraints are built by organizing the above-established models, including the constraint of the nodal power balance in electricity networks, the electrical power transmission limit, the phase angle constraints, the output active power constraint of the generator, the ramping constraints

of CHP and the thermal power units, the electric power output and heating power output of CHP, and electric power output limit of the wind power generator (Equations (25)–(32)).

(3) We choose the heating power of CHP as the benchmark, and express the power supply of CHP as a piecewise linear function about the heating power to achieve the linearization of the CHP electricity–heating coupling curve. Based on the maximum heating power output, and electricity–heating coupling relationship of CHP, we obtain the electric and heating power output constraints of CHP (Equations (33)–(47)). By incorporating various constraints into the constraints of the objective function, the above equation system is combined to obtain the quadratic programming mathematical form of the original optimization scheduling problem.

(4) We solve the quadratic programming problem with the QUADPROG solver. In mathematics, this model belongs to a quadratic programming problem and has a unique solution, so it can be solved using any quadratic programming solver. The QUADPROG solver in MATLAB was used in the study. The solution result was also validated using other software, such as the solver in Python 3.7.

(5) We determine whether the model parameters change. Then, we adjust the parameters, and then obtain different results under different conditions.

(6) We output the final optimization dispatch results. Then, we assess the flexibility (Equations (48) and (49)).

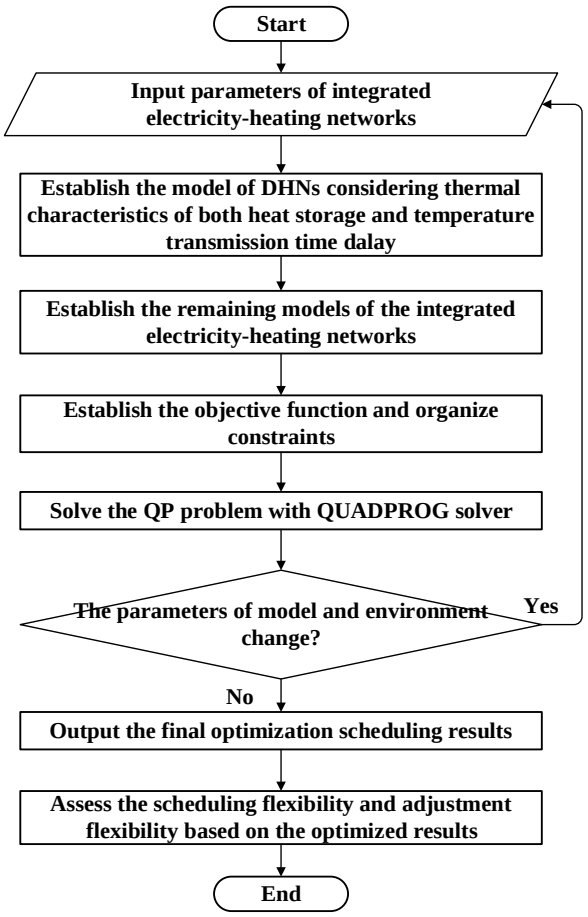

Figure 6. Flowchart of CD and flexibility assessment for the EHS.

5. Case Study

The proposed models consider the thermal characteristics of both TS and temperature TTD for DHNs. The thermal characteristics of the TS of residential buildings are also considered. The optimal dispatch is then carried out. The flexibility assessment

is further conducted. The QUADPROG solver implements the optimal CD model in MATLAB software.

5.1. Six-Node Power Grids with a Six-Node DHN

5.1.1. Structure and Equipment Description

Figure 7 shows the structure of the EHS. The community is a residential building. G1 and G2 are two thermal power plants. Both CHP and WP are constructed at bus 6. The detailed parameters and system structure diagrams of the system are shown in Appendices A–C [28].

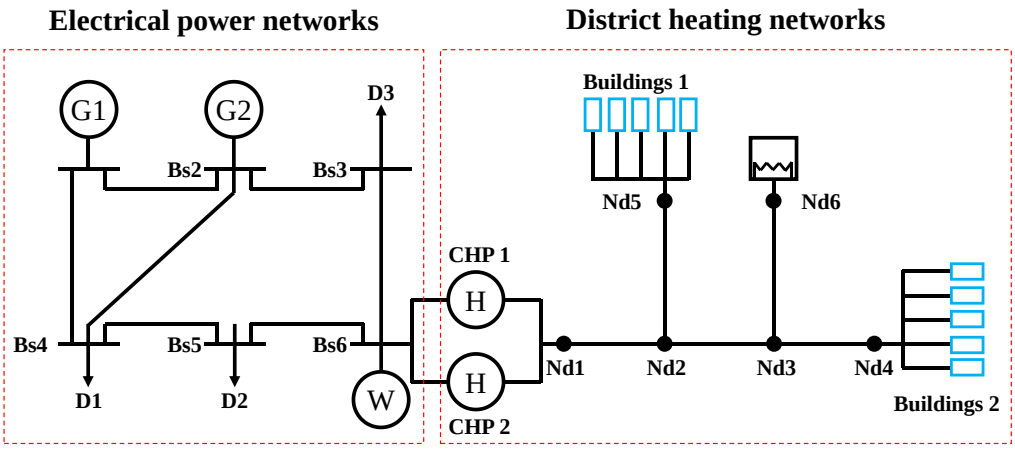

Figure 7. Structure diagram of the six-node power grids with a six-node DHN.

The simulated maximum electrical power load of user loads (in Bus 3, Bus 4, and Bus 5) and the maximum WP (in Bus 6) capacities are 207.5 MW and 28.4 MW, respectively. The electrical power load is dispatched by the power grid company. In Figure 8, the forecasted WP and daily electricity loads are presented [28,31].

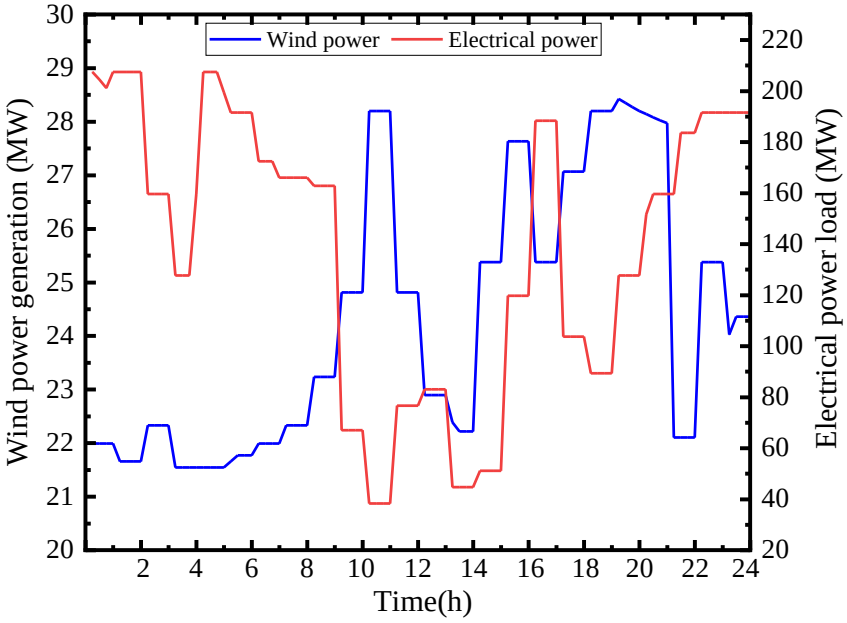

Figure 8. The electricity load and the forecasted WP.

The ambient temperature of outdoor air varies in the range of −17.79 °C to −8.8 °C. The maximum heating loads at node 4 and node 5 (residential buildings) are 23.58 MW and 29.68 MW, respectively. The minimum heating loads at node 4 and node 5 are 5.90 MW

and 12.37 MW, respectively. The ambient temperature, and heating load at nodes 4 and 6 are shown in Figure 9 [28,31].

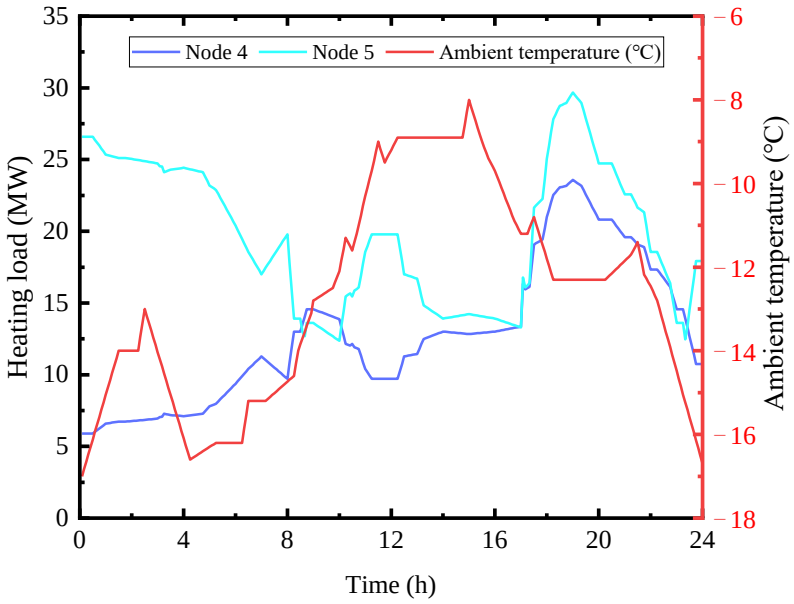

Figure 9. Heating loads of node 4 and node 5 and the ambient temperature of outdoor air.

The comfortable temperature of indoor air is 18 ± 2 °C. In this study, the set standard temperature indoors is °C. Considering the thermal inertia of the walls, the variation range of the indoor temperature is 16~18 °C. The available water temperature is 80 ± 5 °C. The set standard water temperature is 80 °C. To utilize the thermal inertia characteristics of the primary heating pipe networks' TS, the available water temperature range is 75~85 °C. The temperature of the underground soil is −10 °C and is assumed to be constant. Only the thermal characteristics of walls are considered to simplify the heat transmission of buildings.

For the energy system, when there are changes in user electrical power loads, heating loads, and wind power generation, the power grid company adjusts the input or output power from the main power grid to maintain system balance. Compared to the typical load day in this study, the main change is the electrical power input or output from the main power grid.

5.1.2. Descriptions of Four Typical Cases

To study the effects of the thermal inertia characteristics of the DHNs and HPs on the dispatch results, four typical cases are simulated. In each case, the characteristics of the temperature TTD of the DHNs and the heat capacity of buildings are considered. The dispatch time interval is 15 min.

Case 1: CD without considering the heat capacity of DHNs, and without considering the collaborative operation of the HP. In the dispatch, the supply water temperature is adjustable, and the HPO of the HP collaboratively operates with CHP. The standard supply water temperature is 80 °C, which can vary from 75 °C to 85 °C to meet the requirement of optimal dispatch.

Case 2: CD considering the heat capacity of DHNs, and without considering the collaborative operation of the HP. The standard supply water temperature is 80 °C, which can vary from 75 °C to 85 °C to meet the requirement of optimal dispatch.

Case 3: CD without considering the heat capacity of DHNs, and considering the collaborative operation of the HP. In the dispatch, the supply water temperature is kept constant, at 80 °C.

Case 4: CD considering the heat capacity of DHNs and the HP. In the dispatch, the supply water temperature is adjustable, and the HPO of the HP collaboratively operates

with CHP. The standard supply water temperature is 80 °C, which can vary from 75 °C to 85 °C to meet the requirement of optimal dispatch.

5.1.3. Analysis of the Economic Performance

The total cost refers to the fuel cost of CHP at the heat source and thermal power generation units to meet the energy system's power and heating balance consumption; the cost of the DHN refers to the fuel cost of CHP at the heat source and thermal power generation units to meet the heating balance consumption of the energy system, including the heat demand of users and the heat loss transmitted by the heat network; the WP utilized refers to the accumulation of the wind power generated by wind turbines at each moment that is consumed by the grid. The cost comparison between the four cases is shown in Table 2.

Table 2. Costs and utilized WP comparison between four cases.

Cases	Total Cost ($)	Total Cost of DHNs ($)	Total Utilized WP (MWh)
Case 1	11,716	2282	484.43
Case 2	11,514	2207	530.78
Case 3	11,386	2261	571.21
Case 4	11,301	2177	571.21

According to Table 2, the operating costs of the DHN and the whole EHS decrease after using the heat capacity of DHNs without HPs (Case 1 and Case 2); and the operating costs of the DHN and the whole EHS decrease after using the heat capacity of the DHN and HPs at the same time (Case 2 and Case 4). This shows that the heat capacity of the DHN, whether for the system with HPs or without HPs, whether it is a separate DHN or the whole EHS, can reduce the operation cost; the operating costs of the DHN and the whole combined heat and power EHS have decreased after using the HP without TS (Case 1 and Case 3); and the operating costs of the DHN and the whole EHS have decreased after using the heat capacity and HPs at the same time (Case 2 and Case 4,). This shows that the combined use of HPs in the CHP system, whether for the system with or without TS, whether it is a separate heating system or the whole EHS, can reduce the operation cost.

The operation cost of the system decreases the most when both the heat capacity and HPs are used, as in Case 4. However, the decrease in operating costs is small. The WP accommodation of the whole system has increased greatly. In this case, the WP consumption increased from 484.43 MWh to 571.21 MWh, an increase of 17.9%. This shows that it is difficult to reduce the operation cost by using the heat capacity of DHNs or HPs; however, HPs and the heat capacity of DHNs can be used to enhance the flexibility and the consumption of WP.

5.1.4. Analysis of the WP Accommodation

In Case 1, the operation of the EHS does not use HPs or the heat capacity of DHNs. The WP generation and curtailment of the whole system are shown in Figure 10. The periods of wind curtailment are from 9:15~9:30 and from 10:15~15:00, which are mainly due to the large WP generation and small electricity load of users during the period. Because of the large amount of WP curtailment and long duration in the period of 9:15~15:00, the following discussion of WP accommodation under different cases mainly concentrates on this period.

In Figure 11, the supply water temperature comparison is presented. Usually, through the TS of DHNs, the electricity can be temporarily stored in advance in DHNs in the form of thermal energy, to release heat at the stage of excess WP generation, and reduce the power supply of the IES during the stage. The peak load for the EPO can be shifted and the wind power penetration of the EHS can be increased.

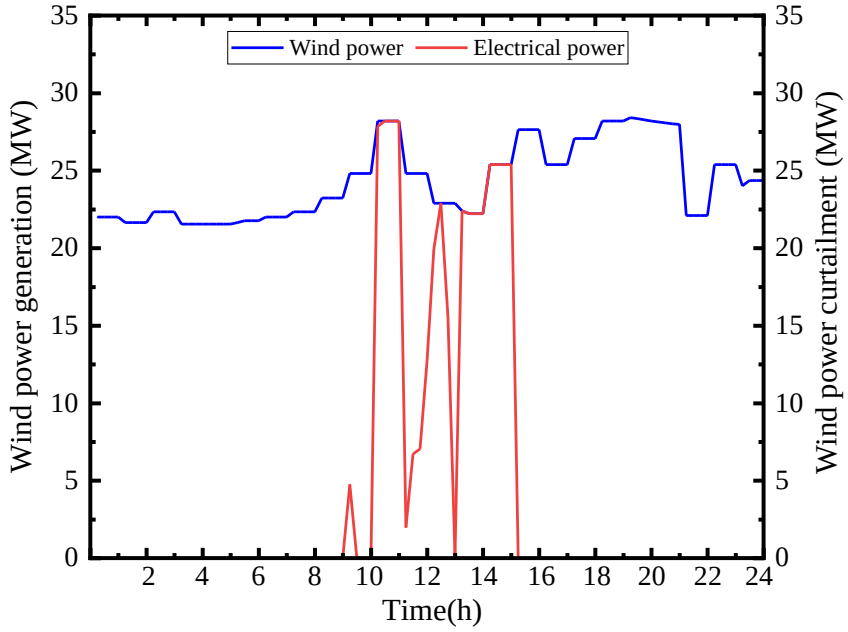

Figure 10. WP generation and the curtailment under Case 1.

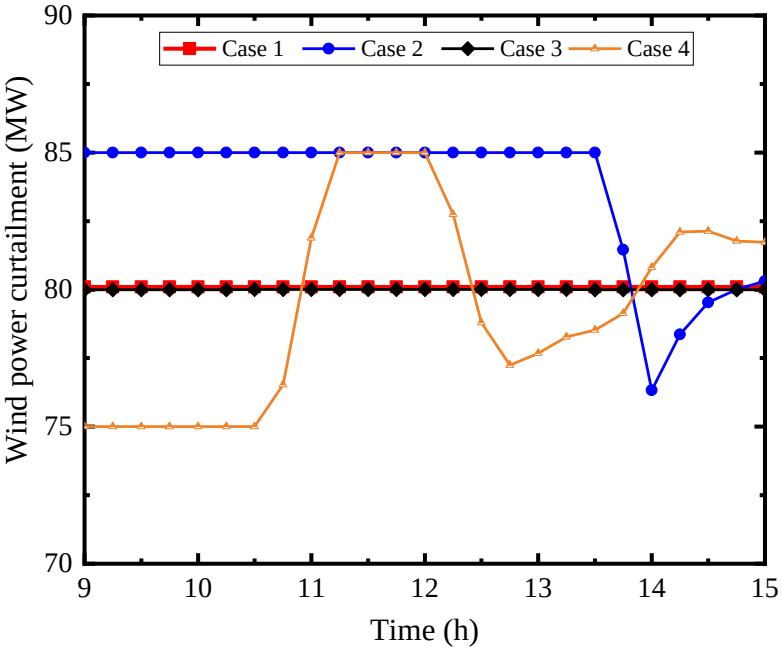

Figure 11. Supply water temperature comparison under four cases.

The WP curtailment comparison under four cases is shown in Figure 12. Combined with Figures 11 and 12, it is found that the WP in Case 2 is smaller than that in Case 1, especially in the period of 10:15–11:00 and 13:30–14:30, which verifies the above conclusion.

In Case 3, the WP curtailment is significantly smaller than that in Case 2, especially in the three periods of 9:00–9:30, 10:15–11:15, and 13:00–15:00. This shows that the HP can enhance the flexibility, and, thus, increase the WP accommodation of the EHS, and the effect is larger than through the heat capacity of DHNs. The main reason is that the value of the heat capacity of DHNs is smaller than the value of the electricity generation of the IES and WP, which makes it easy for DHNs to reach the state of TS saturation.

In the four cases, the order of the WP curtailment is Case 1 < Case 2 < Case 3 = Case 4. On the one hand, it shows that HPs have a better effect than using the heat capacity of DHNs in improving WP consumption; on the other hand, the WP curtailment curves of

Case 3 and Case 4 coincide in this period, which means the effect of using both the HP and heat capacity of DHNs and the effect of using the HP alone is the same for improving the WP consumption. In this circumstance, the heat capacity of DHNs does not have the potential to improve WP consumption. It can be seen from Table 2 that Case 3 and Case 4 have the same WP consumption. This shows that the HP is better than the heat capacity of DHNs for increasing the REE accommodation. When the two are used together, only the HP affects the REE consumption.

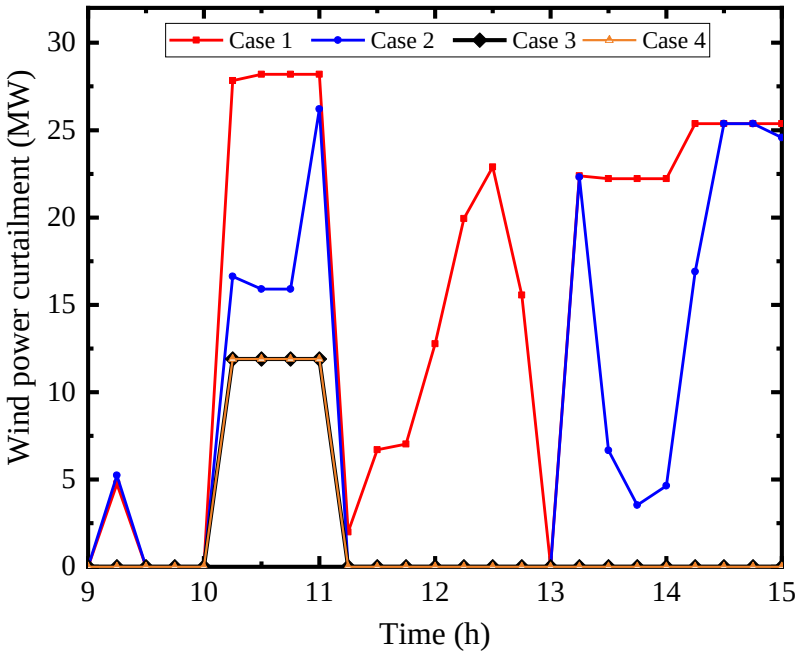

Figure 12. WP curtailment comparison under four cases.

5.1.5. Flexibility Analysis of the IES

According to Figure 5, the heat capacity of the DHN can not only absorb the excess electricity, thus improving the downward flexibility of the IES, but also release the heat stored in the DHN, thus improving the upward flexibility of the IES. However, the HP can only improve the downward flexibility of the IES by consuming electricity, but it cannot release heat or electricity without consuming extra energy. The HP cannot improve the upward flexibility of the IES.

The change in flexibility of the IES is reflected in the output of electricity and heat. To analyze the effect of the change, the EPO of the CU under four cases is assessed and the results are shown in Figure 13. There is a large amount of WP curtailment from 9:00 to 15:00. At this time, the collaborative dispatch of the power generation and heat supply of the IES can reduce the power generation, which will help the electricity networks absorb excess WP and enhance the WP accommodation capacity. Comparing Case 1 and Case 2, it is found that the lower limit of the EPO of the IES can be effectively reduced by using the heat capacity of DHNs, to reduce the EPO power and enhance the accommodation of WP. The dispatch flexibility of the IES in Case 2 is higher than that in Case 1.

The results from Case 2 and Case 3 (or Case 4) mean that the lower limit of the EPO of the IES can be reduced more effectively by using the adjustment capacity of HPs, and the EPO can be greatly reduced, to improve the consumption of WP. Therefore, the heat capacity of DHNs and HPs can improve the downward flexibility of the IES. The improvement of HPs is larger and the effect is better than DHNs.

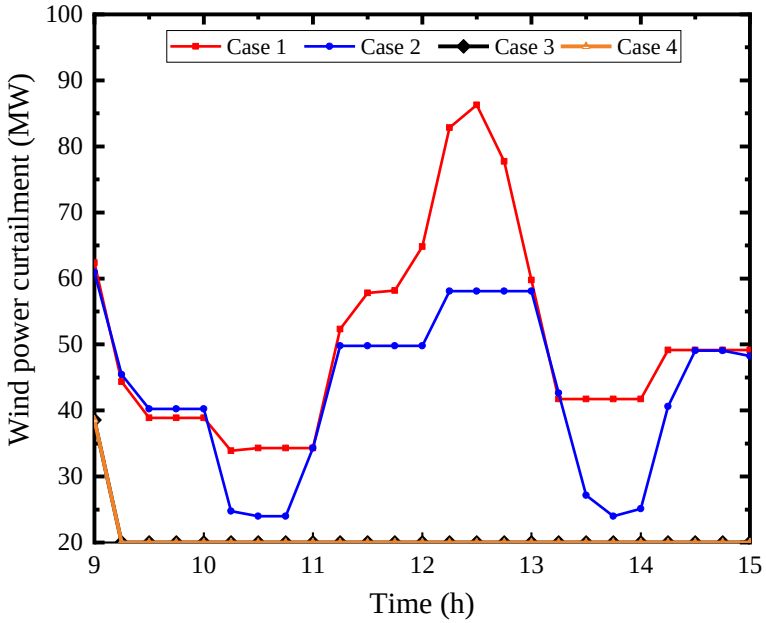

Figure 13. EPO of the CCHTS under four cases.

The comparison of the total EPO and HPO of the CU and HPs under the four cases is shown in Table 3. It can be found that Case 1 and Case 2 do not use HPs, and the heat-to-power ratio during the whole day is close to 1. This indicates that using the TS of DHNs alone has a limited effect on improving the heat-to-power ratio. The heat-to-power ratio is greater than 1.0 due to the use of HPs (Case 3 and Case 4), which indicates that the HP can output less electricity in the circumstance of the same HPO. The use of HPs helps to absorb more WP and cope with the fluctuation of power generation.

Table 3. Comparison of the total EPO and HPO of the CU and HPs under four cases.

Cases	Electricity Output (MWh)	Heating Power Output (MWh)
Case 1	1500.8	1500.6
Case 2	1453.3	1445.3
Case 3	989.5	1486.3
Case 4	984.6	1424.8

5.1.6. Flexibility Assessment

In Figure 14, the flexibility under the four cases is presented. By comparing Case 1 and Case 2, it can be found that, after using the heat capacity of DHNs, the upward flexibility of the system barely increases. Because the heat capacity only transfers the period of the EPO, and increases the upward flexibility of the system in some periods, but decreases the upward flexibility in other periods, the accumulated upward flexibility almost does not increase in one operation cycle. After using the HP, the upward flexibility increases significantly, and the increased range is greater than when using the heat capacity of DHNs alone.

The results from Case 2 and Case 4 mean that the increase in upward flexibility is significant with increasing HP in the circumstance of using TS of DHNs; compared with Case 3 and Case 4, it is found that the increase in upward flexibility is small with the increasing HP in the circumstance of using the heat capacity of DHNs. Therefore, it can be concluded that the upward flexibility improvement of HPs for the EHS is greater than that of the heat capacity of DHNs.

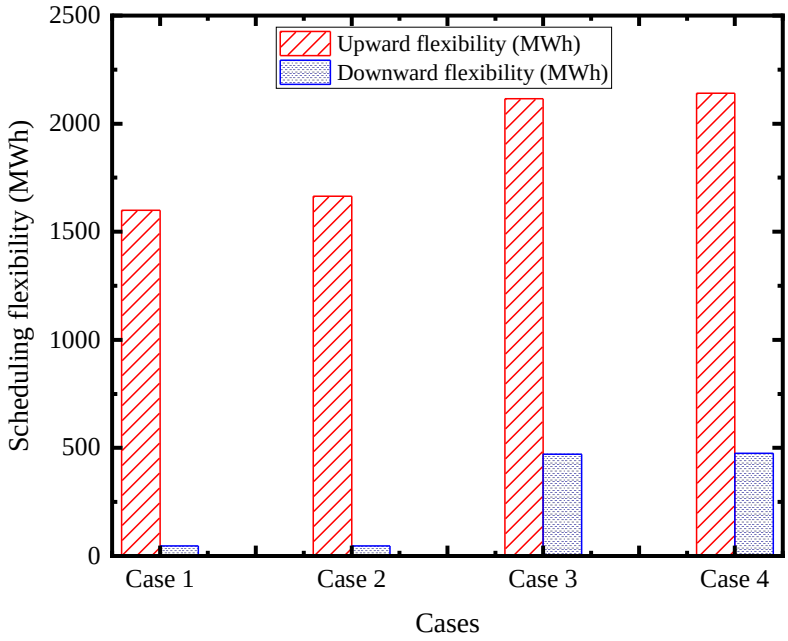

Figure 14. Flexibility of the EHS under four cases.

The results from Case 1 and Case 2 indicate that the downward flexibility changes are minor after using the heat capacity of DHNs because the TS network only transfers the period of the EPO. The influence of heat capacity on downward flexibility is consistent with that of upward flexibility. After using the HP, the upward flexibility is significantly increased, and the maximum is about 10 times that of the original. For the EHS, using the HP can greatly improve downward flexibility.

5.1.7. Flexibility Assessment of the COP of HPs

In this study, the maximum electric power consumption of the HP is 20 MW, and the available ratio, $k_{HP\text{-}CHP}$, is set to 1.0. The influence of the change in COP is analyzed. The minimum EPO of the IES about Q is

$$\left(P^{CU}\right)_{\min} = \begin{cases} 36 - Q(0.3 + 0.5/COP), & 0 \le Q \le 40 \\ 6.8 + Q(0.43 - 0.5/COP), & 40 \le Q \le 40 \cdot COP \\ 6.8 + 0.86Q - (0.86COP + 1) \cdot 20, & Q \ge 40 \cdot COP \end{cases} \quad (50)$$

Then, the discussion can be classified into two circumstances: (1) COP < 1; and (2) COP > 1. For the first circumstance, the HP can be seen as the special electricity–heat conversion device, such as the electric boiler; and the COP can be assumed to be 1.00. For the second circumstance, the HP is the typical electricity–heat conversion device, and the COP can be assumed to be 2.5. Changes in electrical power–heat coupling characteristics along with the COP of HPs are shown in Figure 15.

From Figure 15, it can be concluded that the downward flexibility increases with the COP of HPs. When the HPO power is greater than 40 MW, if the COP of HP is higher than 1.0, the electricity–heating coupling curve is a piecewise linear function. In the beginning, the HPO of HPs gradually increases, which is the curve C_2-C′, and the maximum heat-to-power ratio slowly decreases; then, the HP reaches the upper limit of the rated heating output capacity. At this time, the HPO of the HP no longer increases with the increase in HPO of the CHP, and the maximum heat-to-power ratio of the whole system decreases rapidly. This is the curve C′-B′. If the COP of the HP < 1, the maximum HPO of the HP is always the rated HPO when the HPO of CHP is greater than 40 MW and does not change with increasing HPO. At this stage, the maximum heat-to-power ratio of the whole system decreases rapidly with increasing HPO, which is the curve C_1-B′. When the HPO is large

with the increase in the COP of HPs, the maximum heat-to-power ratio increases, and the downward flexibility increases.

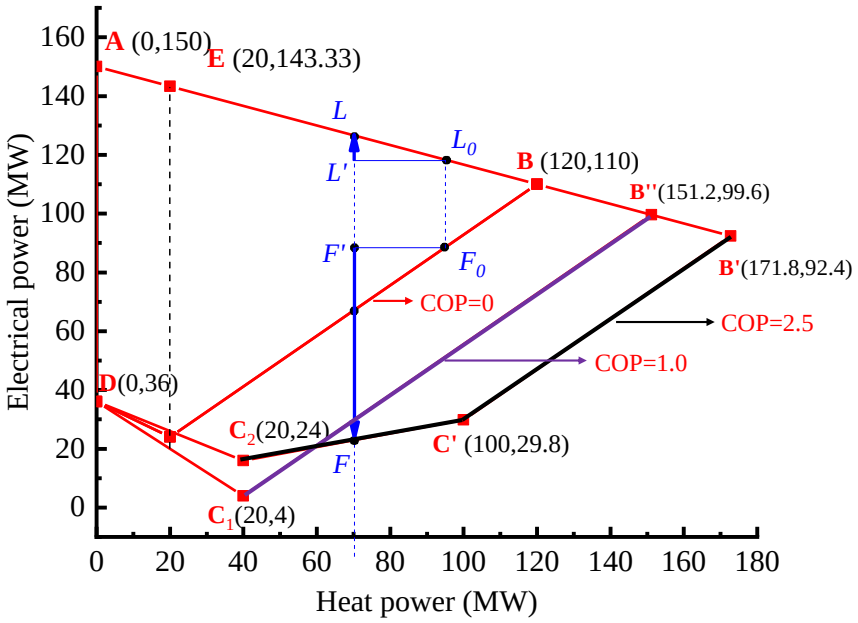

Figure 15. Change of electricity–heating coupling characteristics along with the COP of HPs.

5.2. 39-Node Power Grids with a 12-Node DHN

In this section, the 39-node power grids with a 12-node DHN are constructed as an example for analysis. In Figure 16, the structure diagram of the whole system is presented. The power grids consist of nine thermal power generating units and two wind turbine generator units, which are coupled with a six-node DHN at nodes 25 and 31. The parameters of the DHN are described in Section 5.1. Detailed parameters of the power grids are shown in [31].

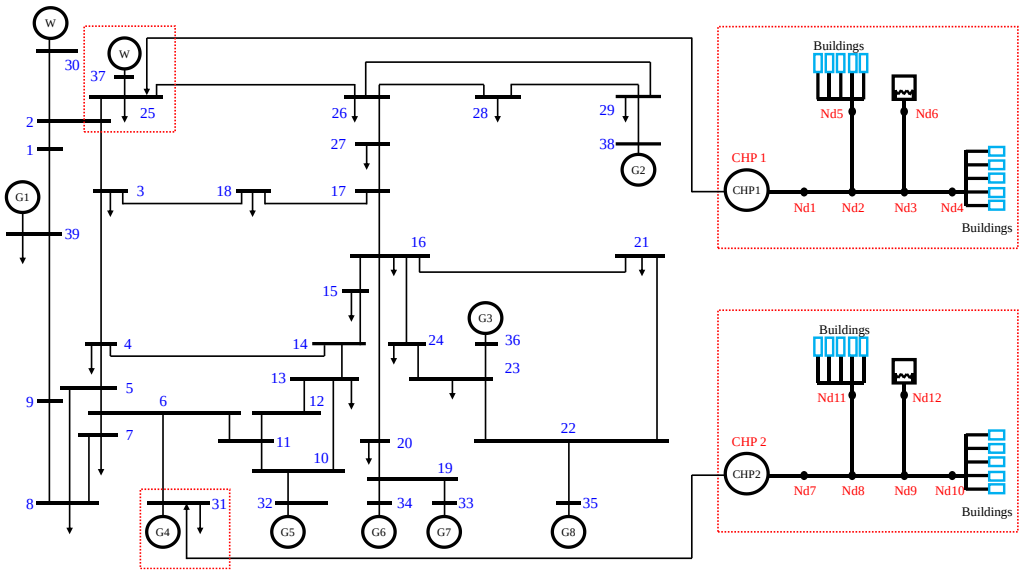

Figure 16. The structure of the 39-node power grids with a 12-node DHN.

It can be found in Section 5.1 that, compared with the use of heating networks and buildings with TS, the flexibility of the whole system has been greatly improved and the renewable energy consumption of the system has been significantly improved after the

use of HPs for electric-to-thermal energy conversion. In this section, the impact of HPs on power supply flexibility and REE accommodation is studied.

5.2.1. Wind Power Accommodation Analysis

The impact of HPs on the REE consumption of the whole system can be obtained. To avoid the impact of TS on the heating network, Case 1 and Case 3 are selected for comparison. Compared with Case 3 and Case 1, the excess wind power consumed by Case 1 and its ratio to the total wind power generation at that time (increased REE accommodation rate) is shown in Figure 17.

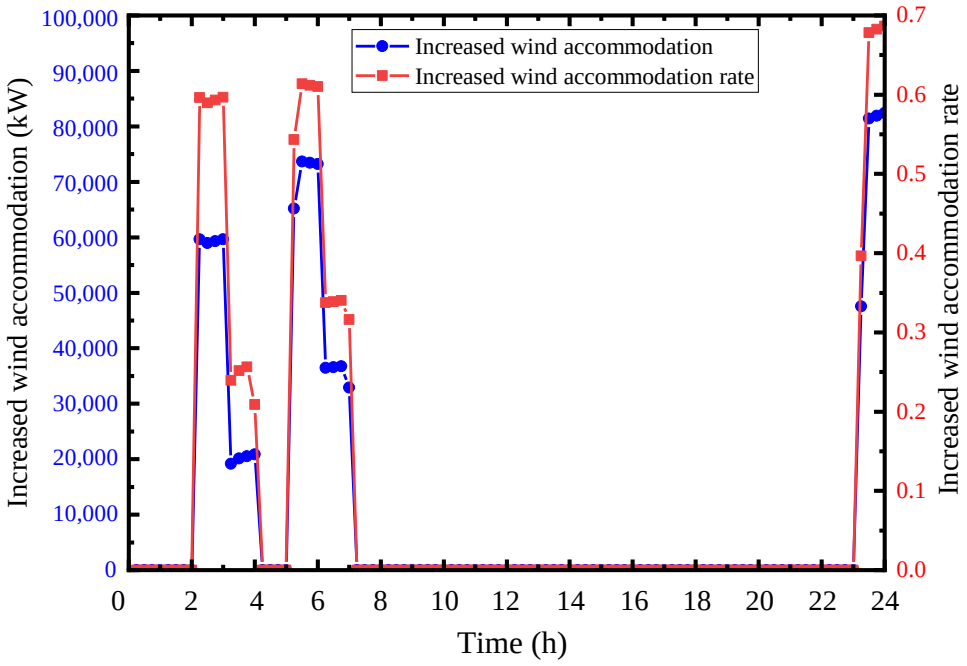

Figure 17. Comparison of the increased wind power accommodation and the increased wind accommodation rate between Case 1 and Case 3.

Due to the low ambient temperature, the COP of heat pumps is generally small. When the COP of the heat pump is 1.50, the overall wind power consumption rate increases from 50.45% to 55.50%, an increase of 10.0%. According to Figure 17, compared with Case 3, in Case 1, from 2:00 to 4:00, from 5:00 to 7:00, and from 23:00 to 24:00, the wind power consumption has increased significantly in these five hours. This shows that the power supply of the CHP unit can be reduced during this period through the role of a heat pump in absorbing wind power as much as possible.

5.2.2. Wind Power Accommodation with COP Change in Electric-to-Thermal Energy Conversion

The COP of the electric–heating conversion equipment has a significant impact on the REE accommodation capacity. When COP < 1.0, the typical electric-to-heating devices are electric heaters; when COP > 1.0, the typical electric-to-heating devices are HPs. COP > 2.0 describes the normal operation range of the heat pump COP; when 1.0 < COP < 2.0, it is only used in some special circumstances.

In Figure 18, the WP adaptation with the COP change in electric-to-heating energy conversion under Case 3 is presented. The WP consumption rate gradually decreases with an increasing COP of electric-to-thermal energy conversion. This is mainly because, with the increase in COP when the same heat power is supplied, the heat pump power consumption decreases, resulting in the excess wind power not being fully consumed. At this time, CHP operates in the left area of C' in Figure 15. When COP > 2.0, with an increasing COP, the decrease in the wind power consumption rate slows down significantly,

which means that the curtailment of WP is close to saturation with the enhancement of the HP COP.

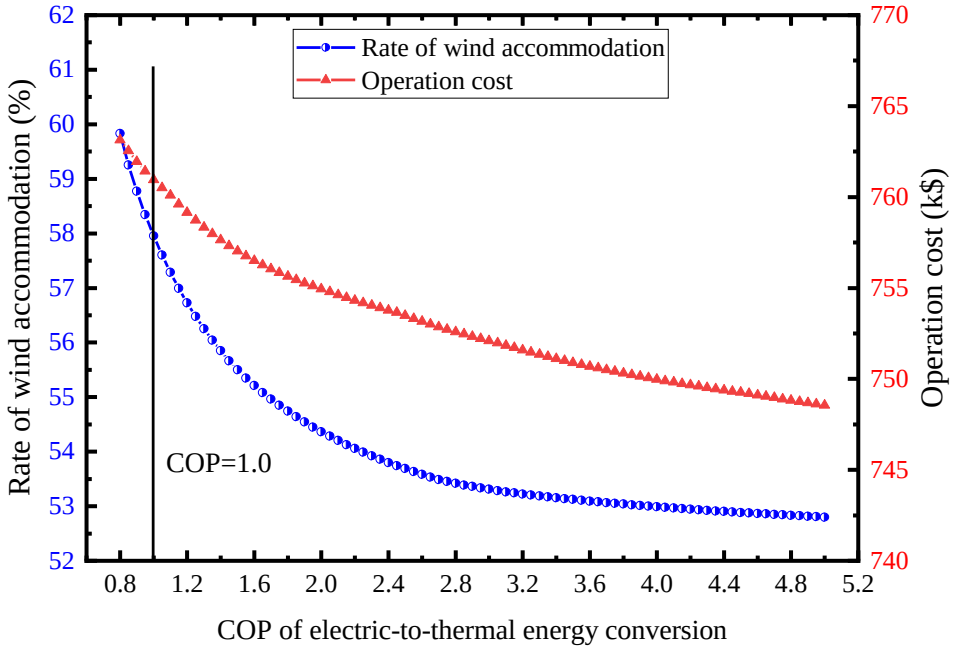

Figure 18. Wind power accommodation with COP changes in electric-to-thermal energy conversion under Case 3.

At the same time, the operating cost decreases with the enhancement of HP's COP. The power consumption is decreased with the enhancement of HP's COP, leading to a decrease in electricity consumption and electricity cost savings.

6. Conclusions

In this paper, the power supply characteristics of a coupled CHP–heat pump–thermal storage system (CCHTS) and the characteristics of renewable energy accommodation are studied. In the case study of four typical circumstances, the results of energy supply flexibility and renewable energy consumption are compared. The conclusions of this study are as follows:

The heat pump is introduced in an electricity–heating IES for system flexible dispatch. By using the HP, the minimum energy supply power can be extended, but the maximum energy supply area will not be changed; by using the TS, the minimum and maximum external energy supply areas will not be changed.

Detailed indices of the IES with coupled HPs are defined. For the coupled multiple-energy system, by analyzing the maximum and minimum energy supply boundary of the energy conversion equipment and establishing the corresponding constraint models, the multi-energy coupling system model and the energy flow optimization method can be combined to improve the capability to respond to highly fluctuating loads with the improved energy supply flexibility.

In the case study of six-node power grids with a six-node DHN, the CCHTS (Case 4) can significantly improve wind power consumption. Compared to the CHP system without HP and TS (Case 1), the WP consumption increased by 17.9%. Both CHP + heat pump (Case 3) and CHP + TS (Case 2) can enhance the power supply flexibility, but the improvement effect of CHP + HP on the power supply flexibility is better than that of CHP + TS. A 7.6% increase in WP consumption is achieved in Case 3. When CHP + HP + TS (Case 4) is used, compared with CHP + HP (Case 3), the flexibility of the system energy supply does not increase significantly. In the case study of 39-node power grids with a 12-node DHN, HPs can increase WP accommodation by 10.0%.

To enhance the flexibility of the EHS and the consumption of REE, a coupled model of HPs with CHP is proposed. In the case study, the maximum upward flexibility increases to 1.34 times that of the original, and the maximum downward flexibility increases to 10.1 times that of the original.

By studying the characteristics of the operating curve of CHP equipment, an optimization scheduling method is proposed for an integrated energy system composed of DHNs, CHP, HPs, and HS, which aims to improve the operational flexibility of the system by co-ordinating the operation of multiple components. This method is based on the flexible electricity–heating supply characteristics of CHP and achieves the coupling of DHNs, CHP, HPs, and HS by flexibly changing the electricity and heat output power within the operating range of the electricity–heating coupling characteristics.

Because the electricity–heating coupling characteristics model of CHP is expressed as a piecewise linear function, the overall model belongs to a quadratic programming model, which has unique mathematical solutions and can be solved using a standardized quadratic programming solver, significantly reducing the modeling complexity and solving difficulty when optimizing schedules for the system.

Considering the characteristics of the energy storage cycle of hydrogen storage, HS, batteries, and other equipment, in future research, it is necessary to study the coupled characteristics between various energy storage devices at different energy storage time scales, to further improve the scheduling flexibility of the integrated system composed of CHP, HPs, and HS, and achieve carbon reduction.

Author Contributions: Conceptualization, D.C. and Z.C.; methodology, D.C.; software, D.C.; data curation, D.C. and Z.C.; writing—original draft preparation, D.C.; writing—review and editing, Z.C.; supervision, Z.C.; project administration, Z.C.; funding acquisition, Z.C. All authors have read and agreed to the published version of the manuscript.

Funding: This research was funded by the National Key Research and Development Program of China, grant number 2018YFB0905000; and the Zhejiang Engineering Research Center for Edge Intelligence Technology and Equipment and the Zhejiang Provincial Department of Education research project, grant number Y202351150.

Data Availability Statement: The data that support the findings of this study are available from the corresponding author upon reasonable request.

Conflicts of Interest: The authors declare no conflicts of interest. The funders had no role in the design of the study; in the collection, analyses, or interpretation of the data; in the writing of the manuscript; or in the decision to publish the results.

Nomenclature

A. Parameters

A	Area of the building
A_j^{window}	The jth wall's whole area of the window
B	Nodal admittance matrix
C_W	Specific heat capacity of water
$C_{w,j}$	The jth wall's heat capacity
D_g	Diameter of pipeline
f^{up}	Upward and downward flexibility reserves
f^{down}	Downward and downward flexibility reserves
k_{delay}	Thermal delay coefficient
L	The pipeline's length
M_{wall}	Total mass of the walls of buildings
m_q	Mass flow rate
$N_{building}$	Number of buildings
P_{it}^{CHP}	Electrical power output of the CHP unit
$P_{i,\max}$	Maximum extrema of the active EPO
$P_{i,\min}$	Minimum extrema of the active EPO

P^{HP}	Consumed electrical power of the HP
Q_{it}^{CUP}	Heating power output of the CHP unit
Q^{HP}	Output heating power of the HP
Q_j^{rad}	Radiative heat flux density
$R_{w,j}$	Thermal resistance
R_{window}	Thermal resistance of the windows
$r_{i,down}$	Downward rates of unit i
$r_{i,up}$	Upward ramp rates of unit i
T_{am}	Ambient temperature
T_i	Temperature at node *i*
$T_{i,su}$	Temperatures of the supply water at node i
$T_{i,re}$	Temperatures of the return water at node i
$T_{s,j}$	Adjacent nodal temperature
$T_{w:j}$	The *j*th wall's temperature
$T_{su,\min}^{HS}$	Minimum temperature of supply water for the heat sources
T^{wall}	Wall's temperature
T_{wj}^{min}	Lower-limit temperature of the wall
t_{delay}	Temperature transmission delay
Δt	Time interval
ΔT	Temperature difference
α_j	Heat-absorbing coefficient
τ	The *j*th wall's heat transfer resistance
λ	Thermal insulation materials' thermal conductivity
δ	Thermal insulation material's thickness
θ	Phase angle
η_{HE}	Efficiency of the heat exchanger
x_{ij}	Reactance of the feeder
Φ	Heating load
B. Abbreviation	
CCHTS	Coupled CHP–heat pump–thermal storage System
CD	Collaborative dispatch
CHP	Combined heat and power
CU	Combined unit
DHN	District heating network
EHS	Electricity–heating system
EPO	Electrical power output
HPO	Heating power output
HP	Heat pump
IES	Integrated energy system
REE	Renewable energy electricity
TS	Thermal storage
TTD	Time transmission delay
WP	Wind power

Appendix A

Table A1. Parameters of the 6-bus electrical power networks.

Branch	*x*
1–2	0.17
1–4	0.258
2–3	0.197
2–4	0.018
3–6	0.037
4–5	0.037
5–6	0.14

Appendix B

Table A2. Parameters of the 6-node DHNs.

Pipeline	Length (m)	Velocity (m/s)	Mass Flow (kg/s)	Diameter (m)
1–2	3200	1.778	502.7	0.60
2–3	2810	1.560	306.4	0.50
2–5	2810	1.562	196.3	0.40
3–4	2800	1.558	110.1	0.30
3–6	2810	1.562	196.3	0.40

Appendix C

Table A3. Parameters of fluid.

Items	Parameters	Value	Unit
ρ	Water density	1000	kg/m^3
C_w	Specific heat of the water	4.2	kJ/(kg·°C)
λ	Thermal conductivity	0.063	W/(m·°C)
h	Heat transfer coefficient between the wall and the air	17.20	W/(m·°C)
T_{am}	The temperature of the soil	−12	°C
η	Heat exchange coefficient	0.92	\
C_{wall}	Specific heat of the wall	0.92	kJ/(kg·°C)
ρ_{wall}	The density of the wall	2500	kg/m^3
M_{wall}	The total mass of the wall	42,139,000	kg

References

1. Dagoumas, A.S.; Koltsaklis, N.E. Review of models for integrating renewable energy in the generation expansion planning. *Appl. Energy* **2019**, *242*, 1573–1587. [CrossRef]
2. Zhang, X.; Wang, Z.; Lu, Z. Multi-objective load dispatch for microgrid with electric vehicles using modified gravitational search and particle swarm optimization algorithm. *Appl. Energy* **2021**, *306*, 118018. [CrossRef]
3. Cai, Q.; Xu, Q.; Qing, J.; Shi, G.; Liang, Q.-M. Promoting wind and photovoltaics renewable energy integration through demand response: Dynamic pricing mechanism design and economic analysis for smart residential communities. *Energy* **2022**, *261*, 125293. [CrossRef]
4. Yang, C.; Li, Z. Distributed Conditional-Distributionally robust coordination for an electrical power and flexibility-enhanced district heating system. *Appl. Energy* **2023**, *347*, 121491. [CrossRef]
5. Li, J.; Fang, J.; Zeng, Q.; Chen, Z. Optimal operation of the integrated electrical and heating systems to accommodate the intermittent renewable sources. *Appl. Energy* **2015**, *167*, 244–254. [CrossRef]
6. Vivian, J.; Quaggiotto, D.; Zarrella, A. Increasing the energy flexibility of existing district heating networks through flow rate variations. *Appl. Energy* **2020**, *275*, 115411. [CrossRef]
7. Vandermeulen, A.; Oevelen, T.V.; Helsen, L.; van der Heijde, B. A simulation-based evaluation of substation models for network flexibility characterization in district heating networks. *Energy* **2020**, *201*, 117650. [CrossRef]
8. Lai, F.; Wang, S.; Liu, M.; Yan, J. Operation optimization on the large-scale CHP station composed of multiple CHP units and a thermocline heat storage tank. *Energy Convers. Manag.* **2020**, *211*, 112767. [CrossRef]
9. Gou, X.; Chen, Q.; Hu, K.; Ma, H.; Chen, L.; Wang, X.-H.; Qi, J.; Xu, F.; Min, Y. Optimal planning of capacities and distribution of electric heater and heat storage for reduction of wind power curtailment in power systems. *Energy* **2018**, *160*, 763–773. [CrossRef]
10. Dai, Y.; Chen, L.; Min, Y.; Mancarella, P.; Chen, Q.; Hao, J.; Hu, K.; Xu, F. Integrated Dispatch Model for Combined Heat and Power Plant with Phase-Change Thermal Energy Storage Considering Heat Transfer Process. *IEEE Trans. Sustain. Energy* **2018**, *9*, 1234–1243. [CrossRef]
11. Yang, H.; Liang, R.; Yuan, Y.; Chen, B.; Xiang, S.; Liu, J.; Zhao, H.; Ackom, E. Distributionally robust optimal dispatch in the power system with high penetration of wind power based on net load fluctuation data. *Appl. Energy* **2022**, *313*, 118813. [CrossRef]
12. Yin, W.; Qin, X.; Huang, Z. Optimal dispatching of large-scale electric vehicles into grid based on improved second-order cone. *Energy* **2022**, *254*, 124346. [CrossRef]
13. Duan, J.; Liu, F.; Yang, Y. Optimal operation for integrated electricity and natural gas systems considering demand response uncertainties. *Appl. Energy* **2022**, *323*, 119455. [CrossRef]
14. Wang, H.; Yin, W.; Abdollahi, E.; Lahdelma, R.; Jiao, W. Modelling and optimization of CHP based district heating system with renewable energy production and energy storage. *Appl. Energy* **2015**, *159*, 401–421. [CrossRef]
15. Fang, T.; Landelma, R. Optimization of combined heat and power production with heat storage based on sliding time window method. *Appl. Energy* **2016**, *162*, 723–732. [CrossRef]
16. Żymełka, P.Y.; Szega, M. Short-term scheduling of gas-fired CHP plant with thermal storage using optimization algorithm and forecasting models. *Energy Convers. Manag.* **2021**, *231*, 113860. [CrossRef]

17. Dai, Y.; Hao, J.; Wang, X.; Chen, L.; Chen, Q.; Du, X. A comprehensive model and its optimal dispatch of an integrated electrical-thermal system with multiple heat sources. *Energy* **2022**, *261*, 125205. [CrossRef]
18. Liu, C.; Wang, C.; Yin, Y.; Yang, P.; Jiang, H. Bi-level dispatch and control strategy based on model predictive control for community integrated energy system considering dynamic response performance. *Appl. Energy* **2022**, *310*, 118641. [CrossRef]
19. Zheng, C.Y.; Wu, J.Y.; Zhai, X.Q.; Wang, R.Z. A novel thermal storage strategy for CCHP system based on energy demands and state of storage tank. *Int. J. Electr. Power Energy Syst.* **2017**, *85*, 117–129. [CrossRef]
20. Romanchenko, D.; Kensby, J.; Odenberger, M.; Johnsson, F. Thermal energy storage in district heating: Centralised storage vs. storage in thermal inertia of buildings. *Energy Convers. Manag.* **2018**, *162*, 26–38. [CrossRef]
21. Chen, X.; Kang, C.; O'Malley, M.; Xia, Q.; Bai, J.; Liu, C.; Sun, R.; Wang, W.; Li, H. Increasing the Flexibility of Combined Heat and Power for Wind Power Integration in China: Modeling and Implications. *IEEE Trans. Power Syst.* **2015**, *30*, 1848–1857. [CrossRef]
22. Saletti, C.; Zimmerman, N.; Morini, M.; Kyprianidis, K.; Gambarotta, A. Enabling smart control by optimally managing the state of charge of district heating networks. *Appl. Energy* **2020**, *283*, 116286. [CrossRef]
23. Jiang, T.; Li, Z.; Jin, X.; Chen, H.; Li, X.; Mu, Y. Flexible operation of active distribution network using integrated smart buildings with heating, ventilation and air-conditioning systems. *Appl. Energy* **2018**, *226*, 181–196. [CrossRef]
24. Wang, D.; Zhi, Y.-Q.; Jia, H.-J.; Hou, K.; Zhang, S.-X.; Du, W.; Wang, X.-D.; Fan, M.-H. Optimal scheduling strategy of district integrated heat and power system with wind power and multiple energy stations considering thermal inertia of buildings under different heating regulation modes. *Appl. Energy* **2019**, *240*, 341–358. [CrossRef]
25. Pan, Z.; Guo, Q.; Sun, H. Feasible region method based integrated heat and electricity dispatch considering building thermal inertia. *Appl. Energy* **2017**, *192*, 395–407. [CrossRef]
26. Li, Y.; Wang, C.; Li, G.; Wang, J.; Zhao, D.; Chen, C. Improving operational flexibility of integrated energy system with uncertain renewable generations considering thermal inertia of buildings. *Energy Convers. Manag.* **2020**, *207*, 112526. [CrossRef]
27. Yao, S.; Gu, W.; Zhou, S.; Lu, S.; Wu, C.; Pan, G. Hybrid Timescale Dispatch Hierarchy for Combined Heat and Power System Considering the Thermal Inertia of Heat Sector. *IEEE Access* **2018**, *6*, 63033–63044. [CrossRef]
28. Li, Z.; Wu, W.; Shahidehpour, M.; Wang, J.; Zhang, B. Combined Heat and Power Dispatch Considering Pipeline Energy Storage of District Heating Network. *IEEE Trans. Sustain. Energy* **2016**, *7*, 12–22. [CrossRef]
29. Zheng, J.; Zhou, Z.; Zhao, J.; Wang, J. Integrated heat and power dispatch truly utilizing thermal inertia of district heating network for wind power integration. *Appl. Energy* **2018**, *211*, 865–874. [CrossRef]
30. Wang, W.; Jing, S.; Sun, Y.; Liu, J.; Niu, Y.; Zeng, D.; Cui, C. Combined heat and power control considering thermal inertia of district heating network for flexible electric power regulation. *Energy* **2019**, *169*, 988–999. [CrossRef]
31. Li, X.; Li, W.; Zhang, R.; Jiang, T.; Chen, H.; Li, G. Collaborative scheduling and flexibility assessment of integrated electricity and district heating systems utilizing thermal inertia of district heating network and aggregated buildings. *Appl. Energy* **2020**, *258*, 114021. [CrossRef]
32. Gu, W.; Wang, J.; Lu, S.; Luo, Z.; Wu, C. Optimal operation for integrated energy system considering thermal inertia of district heating network and buildings. *Appl. Energy* **2017**, *199*, 234–246. [CrossRef]
33. Dai, Y.; Chen, L.; Min, Y.; Chen, Q.; Hao, J.; Hu, K.; Xu, F. Dispatch Model for CHP With Pipeline and Building Thermal Energy Storage Considering Heat Transfer Process. *IEEE Trans. Sustain. Energy* **2019**, *10*, 192–203. [CrossRef]
34. Wu, C.; Gu, W.; Jiang, P.; Li, Z.; Cai, H.; Li, B. Combined Economic Dispatch Considering the Time-Delay of District Heating Network and Multi-Regional Indoor Temperature Control. *IEEE Trans. Sustain. Energy* **2018**, *9*, 118–127. [CrossRef]
35. Feldhofer, M.; Healy, W.M. Improving the energy flexibility of single-family homes through adjustments to envelope and heat pump parameters. *J. Build. Eng.* **2021**, *39*, 102245. [CrossRef]
36. Fitzpatrick, P.; D'ettorre, F.; De Rosa, M.; Yadack, M.; Eicker, U.; Finn, D.P. Influence of electricity prices on energy flexibility of integrated hybrid heat pump and thermal storage systems in a residential building. *Energy Build.* **2020**, *223*, 110142. [CrossRef]
37. Nolting, L.; Praktiknjo, A. Techno-economic analysis of flexible heat pump controls. *Appl. Energy* **2019**, *238*, 1417–1433. [CrossRef]
38. Patteeuw, D.; Henze, G.P.; Helsen, L. Comparison of load shifting incentives for low-energy buildings with heat pumps to attain grid flexibility benefits. *Appl. Energy* **2016**, *167*, 80–92. [CrossRef]
39. Müller, F.L.; Jansen, B. Large-Scale Demonstration of Precise Demand Response Provided by Residential Heating Systems. *Appl. Energy* **2018**, *239*, 836–845. [CrossRef]
40. Kim, E.; Jamal, H.; Jeon, I.; Khan, F.; Chun, S.E.; Kim, J.H. Functionality of 1-Butyl-2,3-Dimethylimidazolium Bromide (BMI-Br) as a Solid Plasticizer in PEO-Based Polymer Electrolyte for Highly Reliable Lithium Metal Batteries. *Adv. Energy Mater.* **2023**, *13*, 2301674. [CrossRef]
41. Khan, F.; Oh, M.; Kim, J.H. N-functionalized graphene quantum dots: Charge transporting layer for high-rate and durable $Li_4Ti_5O_{12}$-based Li-ion battery. *Chem. Eng. J.* **2019**, *369*, 1024–1033. [CrossRef]
42. Chen, D.; Hu, X.; Li, Y.; Wang, R.; Abbas, Z.; Zeng, S.; Wang, L. Nodal-pressure-based heating flow model for analyzing heating networks in integrated energy systems. *Energy Convers. Manag.* **2020**, *206*, 112491. [CrossRef]